

UCRL- 94160
PREPRINT

Optical Properties and Nonradiative Decay
of Sm^{2+} in $\text{CaF}_2\text{-YF}_3$ and $\text{CaF}_2\text{-LaF}_3$ Mixed Crystals

L. L. Chase
Stephen A. Payne
and
Gary D. Wilke

CIRCULATION COPY
SUBJECT TO RECALL
IN TWO WEEKS



This paper was prepared for submittal to the
Journal of Physics C.

February 13, 1986

Lawrence
Livermore
National
Laboratory

This is a preprint of a paper intended for publication in a journal or proceedings. Since changes may be made before publication, this preprint is made available with the understanding that it will not be cited or reproduced without the permission of the author.

DISCLAIMER

This document was prepared as an account of work sponsored by an agency of the United States Government. Neither the United States Government nor the University of California nor any of their employees, makes any warranty, express or implied, or assumes any legal liability or responsibility for the accuracy, completeness, or usefulness of any information, apparatus, product, or process disclosed, or represents that its use would not infringe privately owned rights. Reference herein to any specific commercial products, process, or service by trade name, trademark, manufacturer, or otherwise, does not necessarily constitute or imply its endorsement, recommendation, or favoring by the United States Government or the University of California. The views and opinions of authors expressed herein do not necessarily state or reflect those of the United States Government or the University of California, and shall not be used for advertising or product endorsement purposes.

Optical Properties and Nonradiative Decay of Sm^{2+}
in $\text{CaF}_2\text{-YF}_3$ and $\text{CaF}_2\text{-LaF}_3$ Mixed Crystals *

L. L. Chase, Stephen A. Payne and Gary D. Wilke

Lawrence Livermore National Laboratory

P. O. Box 808

Livermore, California 94550

ABSTRACT

We have obtained the absorption and emission spectra for the Sm^{2+} impurity in the mixed fluorides, $\text{Ca}_{1-x}\text{Y}_x\text{F}_{2+x}$ and $\text{Ca}_{1-x}\text{La}_x\text{F}_{2+x}$. From these spectra we conclude that the Sm^{2+} ions tend to be coordinated by one or more extra F^- ions in addition to the normal eight-fold coordination expected in CaF_2 . Our measurements of the emission lifetime and intensity as a function of temperature lead us to propose that the luminescence quenching of Sm^{2+} in the mixed fluorides is due to a competition between ionization of the $4f^55d$ level with relaxation into the $^5D_0(4f^6)$ emitting state. In addition, the thermal activation energy for Sm^{2+} emission quenching in various alkaline earth halides is consistent with the calculated optical separation of the $4f^55d$ level from the conduction band of the host, lending further support to the ionization mechanism of emission quenching.

*Work performed under the auspices of the U.S. Department of Energy by Lawrence Livermore National Laboratory under Contract No. W-7405-ENG-48.

1. Introduction

Divalent samarium has been of interest to researchers for several decades. Since the divalent state is reasonably stable relative to the trivalent state, it is possible to incorporate Sm^{2+} into a number of crystalline hosts (Alam and DiBartolo 1967, Axe and Sorokin 1963, Dieke and Sarup 1962, Feofilov and Kaplyanskii 1962, Gros et.al. 1981, Kaplyanskii and Feofilov 1964, Lauer and Fong 1976, Valyashko 1977). The strongly allowed $4f^6 \rightarrow 4f^5 5d$ transitions of Sm^{2+} observed in the visible and UV are interesting because they are sensitively affected by the nature of the crystalline environment near the impurity. This, in turn, affects the luminescent properties of these materials, which are known to be largely determined by the relative position of the lowest of the $4f^5 5d$ and the $^5D_0(4f^6)$ excited states (Wood and Kaiser 1962).

The physical properties of the "mixed fluorides" of the general formula $\text{M}_{1-X}\text{Ln}_X\text{F}_{2+X}$ have also been of great interest for some time now (Kaminskii et.al. 1967, 1984a, 1984b, Kaminskii 1967). Here M may be Ca, Sr, Ba or Cd, while Ln may be Sc, Y, La, Lu or any of the trivalent rare earths. If the level of Ln^{3+} doping is kept below ~ 0.4 , the cubic crystal structure of the fluorite lattice is retained in the disordered crystals. Although the exact nature of the Ln^{3+} incorporation is not completely understood, a certain level of disorder is known to be introduced into the system. This property may be useful for Nd^{3+} -solid state lasers because the Nd^{3+} emission lines are substantially broadened when $X=0.1-0.4$ Ln^{3+} . Therefore, the pumping efficiency for broadband pump sources is increased and the peak stimulated emission cross-section is reduced. This smaller cross-section reduces the deleterious effects of amplified spontaneous emission. Also,

the fluoride hosts are expected to have a smaller nonlinear refractive index compared to the oxide-based laser glasses (Kaminski 1985).

In the present work we compare the 4f-4f luminescence and the 4f-5d absorption of our $\text{Ca}_{1-x}\text{Ln}_x\text{F}_{2+x}:\text{Sm}^{2+}$ crystals, where $\text{Ln}=\text{Y}$ or La and $x=.1-.2$, to that of the alkaline earth halides and relate these observations to the structural properties of the $\text{Ca}_{1-x}\text{Ln}_x\text{F}_{2+x}$ mixed fluorides. In Section 3.1, we analyze the absorption and emission spectra of Sm^{2+} to find that the Sm^{2+} ion occupies a fairly well-defined site, rather than the expected statistical distribution of sites at the level of 10% Ln^{3+} doping. Using this structural information we then analyze the emission quenching behavior of Sm^{2+} in the mixed fluorides, as well as in the alkaline earth halides, in Section 3.2. Evidence is found for a mechanism of luminescence quenching of Sm^{2+} in all these fluorides based on the ionization theory of McClure and co-workers (1979).

2. Experimental

The experimental procedures employed are well-known methods and are therefore briefly discussed. The absorption spectra were obtained with a computer controlled Cary 17 spectrophotometer. Excitation of the sample was provided by a harmonic of a Molectron MY-34 YAG laser, or by a YAG-pumped dye laser. The emission spectra were obtained by monitoring the signal from a GaAs photomultiplier tube (PMT) mounted at the exit slit of a Chromatix CT-103 monochromator with a boxcar integrator. The monochromator motor was stepped, and the boxcar output was digitized, with a microcomputer. The emission lifetimes were recorded by connecting the PMT output to either a Tektronix R7912 or a PAR 4203 transient

digitizer, depending on whether the signal duration was less or greater than $\sim 100 \mu\text{s}$, respectively. A computer stored the transients so that they could be mathematically analyzed. The single crystal samples were obtained from Optovac Corporation. The Y and La content was determined by inductively coupled plasma spectrochemical analysis.

3. Results and Discussion

3.1 Absorption and Emission Spectra

In the top frame of Figure 1 the well-known absorption spectrum of $\text{CaF}_2:\text{Sm}^{2+}$ is shown (Wood and Kaiser 1962). The ground state of Sm^{2+} is $4f^6$, so the broad bands arise from the $4f^6 \rightarrow 4f^5 5d$ transitions. Since the Sm^{2+} ions experience an eight-fold coordinated cubic environment, the 5d orbital will be split into e_g and t_{2g} components. To a reasonable approximation we may describe the excited states as the result of a coupling of an e_g or t_{2g} 5d orbital with states of the $4f^5$ core. Thus the 620 and 430 nm bands are due to transitions to the $|e_g, 4f^5 ({}^6\text{H})\rangle$ and $|e_g, 4f^5 ({}^6\text{F})\rangle$ states, respectively, while the 300 nm band is a transition to the $|t_{2g}, 4f^5 ({}^6\text{H})\rangle$ state (Yanase 1976). This sets the crystal field splitting $E(t_{2g}) - E(e_g) = 17000 \text{ cm}^{-1}$. While there are many aspects of the excited states of Sm^{2+} that are not completely understood, this simple picture is generally accepted. We find that the crystal field splittings for SrF_2 and BaF_2 decrease to 15000 and 13000 cm^{-1} , respectively, as expected in view of the increase in the lattice constant.

From traces (b)–(e) of Figure 1, it is apparent that the addition of 10–20% Y^{3+} or La^{3+} results in a drastic change in the

spectrum. By comparing the $\text{CaF}_2:\text{Sm}^{2+}$ spectrum with the others, it is evident that a certain amount of the cubic Sm^{2+} sites remain in the mixed fluorides. The relative amount of these cubic sites decreases with increasing concentration of the trivalent ion. It is also apparent that the fractional occupation of the cubic sites is much lower for a given molar concentration of Y^{3+} than for an equal concentration of La^{3+} .

Spectrum (c), containing 17% Y, exhibits two well-defined peaks at 480 and 330 nm, and a very small amount of the "normal", cubic-site CaF_2 spectrum. Although the complete understanding of all the spectral features of the $\text{Ca}_{0.83}\text{Y}_{0.17}\text{F}_{2.17}:\text{Sm}^{2+}$ sample is not possible, we can reasonably attribute the two major bands as arising from the e_g and t_{2g} orbitals. This gives a crystal field (CF) splitting of 9500 cm^{-1} . Thus the magnitude of the CF splitting has reduced to $(9500/17000) = 56\%$ of the value in CaF_2 .

To understand the decrease in the cubic field splitting we now discuss the structural aspects of trivalent rare earth incorporation into the fluorite lattice. The ideal fluorite structure can be described as follows: the fluoride ions are arranged on a simple cubic sub-lattice while every other eight-fold coordinated site is occupied by a Ca^{2+} ion. Therefore, from the perspective of a Ca^{2+} ion site, the neighboring sites located along the $[110]$ directions are occupied by other Ca^{2+} ions, but the nearest sites along the $[100]$ axes are unoccupied interstitial sites. At the lowest levels of doping of trivalent rare earth (RE) ions into CaF_2 , the RE ion substitutes for a Ca^{2+} ion, while an additional fluoride ion is incorporated into a neighboring interstitial site.

We may therefore expect that the number of excess fluoride ions will be equal to the number of RE ions. When the RE concentration exceeds ~1% it is well known that extensive clustering takes place in CaF_2 , and the actual structure of the RE rich regions becomes quite complex. Prior to discussing the current visualizations of these complex structures, we consider the effects of an ideal crystal containing only statistically distributed interstitial fluorides, as described below.

We perform a simple crystal field (CF) calculation, as described by Griffith (1971), where an eight-fold coordinated Sm^{2+} ion is surrounded by 1, 2 or 3 additional interstitial fluorines (F_i^-). CF theory may be expected to qualitatively describe the orbital splitting pattern and thus provide some physical insight into this problem. In Table 1 the even part of the crystalline potential fields are listed for the "normal" eight-fold cubic environment as well as for 1 to 3 additional F_i^- ions for the particular configuration where no two of the F_i^- ions are on opposite interstitial sites. The odd part of the field has no bearing on the splitting of the 5d manifold and is therefore not listed. Also note that the γ_{40} terms in the CF potentials for the cubic and interstitial fields, denoted as γ_{40}^i and γ_{40} , respectively, are different because of the different Sm-F separations. For the undistorted Sm- F_i separation, we find that $\gamma_{40} = 0.49 \gamma_{40}^i$. We use these potentials along with standard group theory methods to determine the shifts of the energies of the 5d orbitals, as shown in Table 2 (Rotenberg 1959).

The cubic field produces the well-known CF splitting shown in the second column. Now the $\gamma_{20}\langle r^2 \rangle$ term arising from the interstitial fluorines causes a symmetric splitting of the e_g orbitals. This would lower the energy of the lowest $4f^5 5d$ level, contrary to the net upward shift of this level as evidenced by the changes from spectrum (1a) to spectrum (1c). Although the $\gamma_{40}\langle r^4 \rangle$ term for one F_i^- does cause the energy of the e_g orbitals to rise overall, its magnitude seems to be insufficient to explain our results. When the possibility of three F_i^- are examined we see that we are beginning to be able to account for the observed decrease in the CF splitting. In this case, since the $\gamma_{20}\langle r^2 \rangle$ term vanishes, the magnitude of the remaining $\gamma_{40}\langle r^4 \rangle$ term is sufficient to account qualitatively for the experimental results. Although this simple picture of 3 interstitial fluorines neighboring the Sm^{2+} ion in an otherwise undistorted lattice is greatly simplified, it does indicate that the Sm^{2+} ions are probably incorporated into F_i^- -rich submicroscopic regions of the crystal. This is the only mechanism that will cause each Sm^{2+} to be coordinated with several F^- interstitials even at these relatively low Ln^{3+} concentrations. There is considerable theoretical and experimental evidence for the existence of such regions. The cluster calculations of Bendall et.al. (1984) are the most comprehensive to date. These workers have used the HADES program to evaluate the relative stability of a number of different clusters, ranging from a single free interstitial, to a hexamer consisting of six $Ln^{3+}-F_i^-$ pairs. By examining their results several trends become clear. Firstly, larger clusters are

particularly more stable for smaller trivalent ions; viz. Y^{3+} is expected to aggregate much more so than La^{3+} . The spectra of Figure 1 suggest that the Sm^{2+} ions are likely to be incorporated into these aggregates. Secondly, substantial relaxation of neighboring host ions occurs in these clusters. Furthermore, these clusters, including dimers, are energetically favored to "getter" additional F_i ions, even if a n.n. monomer must be dissociated. Andeen et.al. (1977, 1981) believe that they have observed the dielectric relaxations of some of these clusters.

Despite the disorder present in the mixed fluorides Orlov and Stolov (1975) have noted that the luminescence spectra of trivalent RE activators in $(CaF_2)_{1-x}(YF_3)_x$ vary little from $x=0.02$ to 0.60. They conclude that fairly well defined clusters must exist over the entire concentration range. Similarly, Bevan et.al. (1980) and others (Federov et.al. 1974, Kazanskii 1983) have considered the existence of Ln^{3+} -rich superlattices within the CaF_2 structure. In summary, the data of Figure 1 suggest that the Sm^{2+} site in the mixed fluorides is probably a fairly well defined cluster site where one or more extra fluorines, in addition to the usual eight fluorines, are in the immediate neighborhood of the Sm^{2+} ion.

In Figure 2 the absorption spectra at $T=9K$ are shown for the mixed fluorides. The $Ca_{0.83}Y_{0.17}F_{2.17}:Sm^{2+}$ sample provides a "clean" spectrum, since the absorption of the normal CaF_2 sites has been eliminated. Three broad features are seen at 320, 410, and 480 nm. Several sharp, asymmetric features are also observed, which are not found in the spectrum of $CaF_2:Sm^{2+}$. An example of these is the dip near 420 nm in both crystals. These features are assigned

to Fano resonances similar to the type described by Sturge et.al. (1970) for the V^{2+} impurity. These resonances result from the superposition of transitions from the ground state to a sharp level of the $4f^6$ configuration and an overlapping vibronic band of the $4f^55d$ configuration. These resonances, which are not found in CaF_2 , are present in the mixed crystal because the strong odd-parity crystal field due to the interstitial fluorines produces a substantial oscillator strength for the sharp f-f transitions. Thus, this resonance gives evidence for the loss of the inversion centre at the Sm^{2+} site. By multiplying the $4f^6$ energy levels of Eu^{3+} by 0.85 to approximate their energy for Sm^{2+} , we find that the state interfering with the $4f^55d$ band to produce the feature identified by the arrow in Figure 2 must be the $^5L_6(4f^6)$ level (Reisfeld and Jorgensen 1977). The other similar features at shorter wavelengths are difficult to identify without a complete crystal field analysis.

The emission spectra for the two mixed fluoride samples are shown in Figure 3. Although the samples doped with ~20% Ln^{3+} have multiple Sm^{2+} sites, the samples with ~10% Ln^{3+} have predominantly one type of Sm^{2+} emitter; therefore we will discuss primarily lightly doped crystals. The emission spectra result from transitions between levels of the $4f^6$ configuration, which is isoelectronic to Eu^{3+} . The ground states of Sm^{2+} arise from the $^7F_J(4f^6)$ multiplet, where the J=0 through 6 states occur at successively higher energies. The lowest excited state, the emitting level, is the $^5D_0(4f^6)$ state. Therefore the emissions are the result of the $^5D_0 \rightarrow ^7F_J$ transitions. Since the 5D_0 state

does not emit in CaF_2 , these spectra will be compared with those of $\text{SrF}_2:\text{Sm}^{2+}$ where the $^5\text{D}_0$ level emits. The strongest lines of $\text{SrF}_2:\text{Sm}^{2+}$ are listed in Table 3 along with the mixed fluoride results (Wood and Kaiser 1962). It is important to note that the $^5\text{D}_0 \rightarrow ^7\text{F}_1$ line of $\text{SrF}_2:\text{Sm}^{2+}$ is ~100X stronger than any of the other lines, in striking contrast to the mixed fluoride results in Figure 3 and Table 3. The $\Delta J=1$ selection rule has been completely broken by the low symmetry site of the mixed fluorides. We can also see that the splitting of the $^7\text{F}_2$ level by the cubic field of SrF_2 is 383 cm^{-1} , compared to the reduced values of 186 and 259 cm^{-1} for each of the mixed fluorides. Thus the $\text{Ca}_{1-x}\text{Y}_x\text{F}_{2+x}:\text{Sm}^{2+}$ $^7\text{F}_2$ cubic splitting is reduced to 49% of its value, which is in good agreement with the analogous reduction to 56% of the 5d orbital splitting that was determined from the spectra of Figure 1.

The $^7\text{F}_1$ level is also split by the non-cubic crystal field in the mixed fluoride crystals. However, the average energy of the two $J=1$ levels for the Y^{3+} - and La^{3+} -doped samples is 256 and 249 cm^{-1} , quite close to the SrF_2 value of 263 cm^{-1} . Since any point group of symmetry lower than octahedral will split the $J=1(T_{1g})$ level, it is difficult to derive additional structural information from the $^7\text{F}_1$ splitting.

We now summarize our basic structural conclusions from the analysis of the absorption and emission spectra of the Sm^{2+} ion in the mixed fluorides. The reduced values of the crystal field splitting of both the 5d and the $^7\text{F}_2$ levels, coupled with the knowledge that the mixed fluorides have an excess fluorine content,

lead us to believe that the Sm^{2+} ion is coordinated by at least one extra F^- in addition to the normal eight-fold coordination. Three such interstitial fluorines give the best accounting for the changes in the crystal field; however, the possible additional effects of distortions produced by the disorder are too uncertain to precisely specify the character of the Sm^{2+} site. Furthermore, the observation of the Fano resonances in Figure 2 indicates that the inversion center at the Sm^{2+} site has been destroyed by the extra F^- ion(s). The emission spectrum of Figure 3 shows that the Sm^{2+} site in the $\text{Ca}_{0.91}\text{Y}_{0.09}\text{F}_{2.09}$ and $\text{Ca}_{0.90}\text{La}_{0.10}\text{F}_{2.10}$ samples are qualitatively the same, although they differ in their precise structural detail. This structural information will be used as our initial input into the analysis of the emission lifetimes in Section 3.2.

3.2 Emission Lifetimes

As is often the case for impurity ions in crystals, the mechanism for quenching of the emission with increasing temperature is poorly understood. One would ideally like to utilize several quantifiable properties of the host and of the impurity in order to predict the emission efficiency as a function of temperature for a given host/impurity system. We believe that we have made some important progress in this area for the Sm^{2+} impurity.

In Figure 4 the emission lifetime and intensity are plotted as a function of temperature. The behavior of the $\text{Ca}_{0.91}\text{Y}_{0.09}\text{F}_{2.09}:\text{Sm}^{2+}$ sample is unusual in that the intensity steadily diminishes as the temperature is raised, while the lifetime

of the 5D_0 emitting state remains constant from 10 to 230K. A similar dependence is observed for the $\text{Ca}_{0.90}\text{La}_{0.10}\text{F}_{2.10}$ host. Now, the Sm^{2+} ion is initially excited via the $4f^6 \rightarrow 4f^5 5d$ transition, and then it relaxes to the lowest excited state, the $^5D_0(4f^6)$ level in this case, before it emits. It is reasonable to suspect that the decrease in quantum efficiency evidenced by the data in Figure 4 results from the competition for nonradiative decay from the lowest $4f^5 5d$ level; part of the Sm^{2+} ions relax to the $^5D_0(4f^6)$ level where they participate in the emission process, while the rest relax nonradiatively to the 7F ground state. However, a direct nonradiative transition to the ground state would have a negligible influence on the quantum efficiency. This is because nonradiative transition rates decrease very rapidly as the magnitude of the energy gap between the initial and final states increases. Thus, the nonradiative decay rate to the 5D_0 excited state must be orders of magnitude larger than that to the 7F ground term, and all of the energy is expected to relax into the 5D_0 state (Struck and Fonger 1975). As a result, direct decay to the ground state cannot explain the data of Figure 4, and we must consider another mechanism.

We have established in Section 3.1 that the Sm^{2+} environment is coordinated by extra F^- ions. Even if the trivalent RE ion is in the next coordination shell, there will be a net increase in the negative potential at the Sm^{2+} site. This, together with the decreased crystal field splitting of the 5d electron will raise the energy of the lowest $4f^5 5d$ level of the Sm^{2+} ion, and potentially place the $4f^5 5d$ excited state into the conduction band (CB) of the

host. If the lowest $4f^55d$ level were degenerate with the CB it would be possible for Sm^{2+} to ionize upon excitation. This ionization of the $4f^55d$ state could be the process that is competing with relaxation into the $^5D_0(4f^6)$ level. We briefly mention that each of the different sites of the samples heavily doped with Ln^{3+} exhibit different quenching behavior as one would expect from the model presented above due to the sensitivity of the Sm^{2+} energy levels to the number of neighboring F^- ions.

To consider this possibility further we re-examined the Sm^{2+} emission lifetimes for the CaF_2 , SrF_2 (Bonch-Bruevich et.al. 1978), BaF_2 (Bonch-Bruevich et.al. 1975), and $SrCl_2$ (Axe and Sorokin 1963) hosts. For $CaF_2:Sm^{2+}$ the lowest excited state is derived from the $4f^55d$ manifold. As evidenced by the constant lifetime from 10 to 150K in Figure 5, it is clear that the radiative lifetime of this $4f^55d \rightarrow 4f^6$ transition is 1.38 μs . For all the other hosts the $^5D_0(4f^6)$ level is energetically lower than the $4f^55d$ state. Since the 5D_0 lifetime is on the order of several milliseconds, the radiative rate, k_{rad} , must include the rate from the lowest $4f^55d$ levels, which can be thermally populated. Thus, in the absence of quenching,

$$k_{rad} = \frac{p_f + (g_d/g_f) \cdot p_d \cdot \exp(-E_{d-f}/kT)}{1 + (g_d/g_f) \cdot \exp(-E_{d-f}/kT)} \quad (1)$$

where p_f and p_d are the emission rates of the 5D_0 and $4f^55d$ states, respectively, g_f and g_d are their degeneracies, and E_{d-f} is the $4f^55d - ^5D_0$ energetic separation.

The $\text{SrCl}_2:\text{Sm}^{2+}$ system does not exhibit emission quenching and therefore can be fit to Equation 1. The value of E_{d-f} is determined spectroscopically to be 566 cm^{-1} , and we take $p_d = (1.38 \text{ } \mu\text{sec})^{-1}$ from the $\text{CaF}_2:\text{Sm}^{2+}$ data to limit the number of adjustable parameters. From the low temperature data we find that $p_f = (16.1 \text{ msec})^{-1}$. We are then able to fit the lifetime data of Figure 5 with $(g_d/g_f) = 2.3$. These same values of $p_d = (1.38 \text{ } \mu\text{s})^{-1}$ and $(g_d/g_f) = 2.3$ will be used for all of the alkaline earth halides (see Table 4). Because the value of E_{d-f} is determined independently from spectroscopic data and this activation energy is the most important parameter determining k_{rad} , our fitting procedure should be a reasonable approximation for calculating the radiative decay rate of the alkaline earth fluorides.

The emission intensity is known to quench below room temperature for Sm^{2+} in all of the alkaline earth fluorides. As a result, an additional term must be added to describe the overall emission rate,

$$k = k_{\text{rad}} + k_{\text{nr}} \quad (2)$$

where the non-radiative emission rate is

$$k_{\text{nr}} = A_{\text{nr}} \cdot \exp (-E_{\text{nr}}/kT) \quad (3)$$

If we assume that $A_{\text{nr}}(\text{CaF}_2) = A_{\text{nr}}(\text{SrF}_2)$ and fit the data in Figure 5 we find that $E_{\text{nr}} = 0.279 \text{ eV}$ for CaF_2 and 0.206 eV for SrF_2 and $A_{\text{nr}} = 10^{12} \text{ s}^{-1}$ (see Table 4 for the other parameters). We prefer to use the same pre-exponential factor for both crystals since the major physical difference is expected to involve the activation energy. The dotted lines in Figure 5 indicate what the lifetime of the crystals would have been in the absence of non-radiative quenching, (i.e., $k = k_{\text{rad}}$). By letting the values of

A_{nr} and E_{nr} vary independently for $BaF_2:Sm^{2+}$ we find $E_{nr}=0.14$ eV. (We will consider this again later.) Table 4 contains a complete listing of all the parameters used to fit the data in Figure 5.

Physically, we may interpret E_{nr} as the thermal energy required to promote an electron from the lowest excited state of Sm^{2+} to the CB, resulting in ionization. To determine the thermal energy separation of the lowest $4f^55d$ state from the CB, we must subtract E_{f-d} from E_{nr} .

$$E_{therm} = E_{nr} - E_{d-f} \quad (4)$$

These results are tabulated in Table 5. We can also calculate the optical threshold energy for photoionization with the theory of Pedrini, McClure and Anderson (1979). This energy represents the vertical energy separation of the $4f^55d$ state from the CB and cannot be directly compared with the thermal value that we have experimentally determined. However, the changes in the thermal and optical energies from host to host should be correlated. Pedrini, et.al. (1979) have demonstrated that the photoionization threshold, E_{PI} , can be calculated with

$$E_{PI} = I - E_M - \Delta E_M - E_{pol} \quad (5)$$

where I is the ionization potential of the impurity ion, E_M is the electrostatic potential energy at the metal site for the perfect crystal, ΔE_M is the correction for the previous term due to the distortion introduced by the impurity, and E_{pol} is the polarization energy due to the removal of an electron at the metal site. Pedrini et.al. (1986) have tabulated these calculations for all of the

divalent RE ions in the alkaline earth fluorides. Using their results, and the equation

$$E_{\text{opt}} = E_{\text{PI}} - E_{\text{d-f}} \quad (6)$$

we can theoretically determine the optical separation of the lowest $4f^5 5d$ state from the CB. These results are also in Table 5. It is apparent that there is a correlation between E_{opt} and E_{therm} . In addition, it is recognized that the vertical (optical) energy separation is normally larger than the thermal value. For example, according to Pekar's theorem, the optical energy required to release a strongly coupled polaron from its polarization well is equal to three times the result obtained by thermal excitation (Lemmon and Devreese 1973, Ascarelli and Stulen 1975). Although this physical situation is not directly applicable, the result is approximately the right order of magnitude.

It is apparent that the lowest $4f^5 5d$ level of Sm^{2+} may actually be located in the CB for BaF_2 . This explains why the emission quantum yield of BaF_2 is low, even at $T=4\text{K}$ (Wood and Kaiser 1962). Note that both the values of A_{nr} and E_{nr} were allowed to vary for BaF_2 , while we set $A_{\text{nr}}(\text{CaF}_2) = A_{\text{nr}}(\text{SrF}_2)$. This is because the lowest $4f^5 5d$ level of Sm^{2+} is in the CB for BaF_2 , while it is well below it for CaF_2 and SrF_2 , resulting in two qualitatively different physical situations.

In the case of $\text{SrCl}_2:\text{Sm}^{2+}$, quenching was not observed up to 450K, so we can only set a lower limit of $E_{\text{therm}} > 0.8 \text{ eV}$. For comparison, we calculate E_{PI} for SrCl_2 by scaling the SrF_2 values of E_{M} and E_{pol} for the increased lattice constant of SrCl_2 and the greater polarizability of Cl^- vs. F^- . We find

that $E_{\text{opt}} \approx 3.8$ eV. Therefore, both E_{therm} and E_{opt} are larger for the chloride compared to the fluorides, see Table 5.

The values of E_{PI} for the mixed fluorides were calculated by using $E_{\text{PI}}(\text{CaF}_2)$ and including the potential that would result from an additional F^- in the center of the interstitial site along with the substitution of a neighboring Ln^{3+} for a Ca^{2+} ion. In the light of the discussion of Section 3.1, this model will provide a lower limit for the added potential seen by a Sm^{2+} ion in the fluoride rich region. We find that $E_{\text{opt}} < -0.2$. This is in agreement with the data in Figure 4, which indicate that the $4\text{f}^5 5\text{d}$ level is in the CB, or that $E_{\text{therm}} < 0.0$. The mixed fluoride results are listed in Table 5.

The question of what happens to the electron following ionization has not been resolved. The electron that is ionized may immediately return to the ground state of the same Sm, thereby eliminating any luminescence. Alternatively it may be trapped somewhere else in the crystal (such as at Sm^{3+} ion). It may also return at a later time. We have not investigated these effects; however, the photoionization measurements of Pedrini et.al. (1986) and the hole-burning experiments of MacFarlane and Shelby (1984) do provide evidence for the photoionization process.

To summarize, we conclude that the emission quenching of Sm^{2+} in the alkaline earth halides is largely determined by the relative position of the lowest $4\text{f}^5 5\text{d}$ level and the CB of the host. Two independent analyses provided support for this idea. Firstly, we observed that the emission intensity of Sm^{2+} in the mixed fluorides decreases with increasing temperature, while the emission lifetime

remains constant. Since this effect could not be rationalized within the framework of a configuration coordinate diagram, we postulated that the relaxation from the $4f^55d$ level to the $^5D_0(4f^6)$ emitting state is competing with direct ionization from the $4f^55d$ state. We then compared the experimental thermal energies for Sm^{2+} emission quenching in the alkaline earth halides to the calculated optical ionization energies, and found that the observed trends could be accounted for.

4. Conclusion

Numerous investigations of trivalent RE ions doped into the mixed fluoride hosts have been conducted. The present work is the first investigation of a divalent RE in these materials. The absorption and emission spectra were used, along with various structural studies of the mixed fluorides from the literature, to determine that the Sm^{2+} site symmetry is lowered by the introduction of additional F^- ion(s) into its immediate environment. We determined that the cubic splitting is substantially reduced for the mixed fluorides, compared to CaF_2 , and also that a significant odd-parity component is present in the crystal field. We propose that the net increase in the negative potential due to the excess F^- ions raises the Sm^{2+} energy levels enough to push the $4f^55d$ excited state into the CB of the host. The observation of a constant emission lifetime along with a diminishing emission intensity from lower to higher temperature is cited as evidence for competition between an ionization process from the $4f^55d$ level and relaxation into the emitting $^5D_0(4f^6)$ state. The experimental thermal activation energy for emission quenching of Sm^{2+} in various alkaline earth halides

correlates well with the calculated vertical energy separation of the $4f^5 5d$ state and the CB of the host, providing good support for our ionization model.

Figure 1. Room temperature absorption spectra of Sm^{2+} in CaF_2 and in the mixed fluorides.

Figure 2. Absorption spectra at $T=9\text{K}$ for Sm^{2+} in the Y- and La-mixed fluorides.

Figure 3. $^5\text{D}_0 \rightarrow ^7\text{F}_J$ emission spectra of Sm^{2+} in the mixed fluorides, uncorrected for the response of the detector excited at 355 nm. The J-value for the final state is indicated.

Figure 4. Emission intensity and lifetime measurements as a function of temperature for Sm^{2+} in the mixed fluorides, excited at 355 nm.

Figure 5. Emission lifetime measurements as a function of temperature for Sm^{2+} in the indicated alkaline earth halides. The solid line is a theoretical fit to the data, including the effect of non-radiative quenching; the dotted line is the calculated radiative lifetime.

Table 1
Cubic and Interstitial Fluorine Crystal Field Potentials

environment	field in γ_M^L (even part)
cubic*	$-(4\sqrt{7}/9) \cdot \gamma_{40}' r^4 [\sqrt{7} Y_0^4 + \sqrt{5} (Y_4^4 + Y_{-4}^4)]$
1 F_1^- †	$\gamma_{20} r^2 Y_0^2 + \gamma_{40} r^4 Y_0^4$
2 F_1^-	$-\gamma_{20} r^2 Y_0^2 + (3/4) \cdot \gamma_{40} r^4 Y_0^4$ $+(\sqrt{35}/4) \cdot \gamma_{40} r^4 (Y_4^4 + Y_{-4}^4)$
3 F_1^-	$(16\sqrt{7}/81) \cdot \gamma_{40} r^4 [\sqrt{7} Y_0^4 + \sqrt{5} (Y_4^4 + Y_{-4}^4)]$

* $\gamma_{40}' = \frac{\sqrt{4\pi} k e^2}{3R'^5}$, where R' = the Sm-n.n.F distance, r is the 5d electron radius, and $k=9 \times 10^9 \text{ m}^{-2} \text{ C}^2 \text{ N}$

† $\gamma_{40} = \frac{\sqrt{4\pi} k e^2}{3R^5}$, $\gamma_{20} = \frac{\sqrt{4\pi} k e^2}{\sqrt{5} R^3}$, where R = the Sm- F_1 distance.

Table 2*
Cubic and Interstitial Fluorine (int.F⁻) Crystal Field Splittings

3d orbital	cubic $\gamma_{40}'\langle r^4 \rangle$	1 int. F ⁻		2 int. F ⁻		3 int. F ⁻	
		$\gamma_{20}\langle r^2 \rangle$	$\gamma_{40}\langle r^4 \rangle$	$\gamma_{20}\langle r^2 \rangle$	$\gamma_{40}\langle r^4 \rangle$	$\gamma_{20}\langle r^2 \rangle$	$\gamma_{40}\langle r^4 \rangle$
t_{20}	0.50	-0.18	0.04	0.18	-0.26	0	-0.22
$t_{2\pm 1}$	0.50	0.09	-0.16	-0.09	-0.06	0	-0.22
$e_{g\theta}$	-0.75	0.18	0.24	-0.18	0.09	0	0.33
$e_{g\varepsilon}$	-0.75	-0.18	0.04	0.18	0.29	0	0.33

*See Table 1 for definition of γ_{LO} ; units are in $\gamma_{LO}\langle r^n \rangle$ as indicated.

Table 3
Splitting of 7F_J Ground State (cm^{-1})

J	SrF_2	$\text{Ca}_{0.91}\text{Y}_{0.09}\text{F}_{2.09}$	$\text{Ca}_{0.90}\text{La}_{0.10}\text{F}_{2.10}$
0	0 [14616]	0 [14630]	0 [14670]
1	263 (278 in BaF_2)	192, 320	153, 344
2	652, 1035	744, 930	753, 1012
3	1476	1490	1531
4	2266	2053, 2234 2329, 2446	2105, (2252, 2292) 2369, 2465

Table 4.
Parameters used to fit the lifetime data in Figure 5.

Crystal	$1/p_d$ (μs)	(g_d/g_f)	$1/p_f$ (ms)	E_{d-f_1} (cm^{-1})	A_{nr_1} (s^{-1})	E_{nr} (eV)
$SrCl_2$	1.38	2.3	16.1	566	(10^{12})	>0.9
CaF_2	1.38	2.3	-	-	10^{12}	0.279
SrF_2	1.38	2.3	12.6	436	10^{12}	0.206
BaF_2	1.38	2.3	12.9	900	3×10^{10}	0.14

Table 5
Experimental Thermal Excitation Energies and Calculated Optical
Excitation Energies from the $4f^5 5d$ State of Sm^{2+} to the CB

Crystal	E_{therm} (eV)	E_{opt} (eV)
CaF_2	0.28	1.9
SrF_2	0.15	1.2
BaF_2	0.03	0.1
SrCl_2^*	>0.8	~3.8
$\text{Ca}_{1-x}\text{Y}_x\text{F}_{2+x}^\dagger$	<0.0	<-0.2
$\text{Ca}_{1-x}\text{La}_x\text{F}_{2+x}^\dagger$	<0.0	<-0.2

* E_{pol} and E_{M} values for SrF_2 were scaled for Cl^- vs. F^- , and for the larger lattice constant.

† Calculated using the E_{PI} value for CaF_2 , and assuming an extra F^- at the [100] interstitial site and a Ln^{3+} ion at the [110] metal site.

References

- Alan A S M and DiBartolo, 1967, J. Chem. Phys. 47, 3790-3801.
- Andeen C, Link D and Fontanella J, 1977 Phys. Rev. B 16, 3762-7.
- Andeen C, Fontanella J J, Wintergill M C, Welcher P J, Kimble R J and Matthews G E, 1981, J. Phys. C:Solid State 14, 3557-75.
- Ascarelli G and Stulen R H, 1975 Phys. Rev. B 11, 4045-8.
- Axe J D and Sorokin P P, 1963 Phys. Rev. 130, 945-52.
- Bendall P J, Catlow C R A, Corish J and Jacobs P W M, 1984, J. Solid State Chem. 51, 159-69.
- Bevan D J M, Greis O and Straehle J, 1980, Acta. Cryst. A36, 889-91.
- Bonch-Bruevich V A, Ignatev I V and Ovsyankin V V, 1978 Opt. Spectrosc. 44, 429-32.
- Bonch-Bruevich V A and Ovsyankin V V, 1975 Sov. Phys. Solid State 17, 587-8.
- Dieke G H and Sarup R, 1962 J. Chem. Phys. 36, 371-7.
- Federov P P, Izotova O E, Alexandrov V B and Sobolev B P, 1974 J. Solid State Chem. 9, 368-74.
- Federov P P and Kaplyanskiĭ A A, 1962 Opt. Spectrosc. 12, 272-7.
- Griffith J. S. 1971, The Theory of Transition-Metal Ions (Cambridge, University Press).
- Gros A, Gaume F and Gacon J C, 1981 J. Solid State Chem. 36, 324-30.
- Kaminskiĭ A A, Voronko Y K and Osiko V V, 1967a Phys. Stat. Sol. 21, K17-21.
- Kaminskiĭ A A, 1967b, Phys. Stat. Sol. 20, K51-4.
- Kaminskiĭ A A, Sobolev B P, Z I Zhmurova and Sarkisov S E, 1984a Inorg. Materials 20, 759-60.

- Kaminskii A A, Zhmurova Z I, Lomonov V A and Sarkisov S E, 1984b Phys. Stat. Sol. (B) 84, K81-4.
- Kaminskii A A, 1985 Phys. Stat. Sol. (A) 87, 11-57.
- Kaplyanskii A A and Feofilov P P, 1964 Opt. Spectrosc. 16, 144-149.
- Kazanskii S A, 1983 JETP Lett. 38, 521-5.
- Lauer H V and Fong F K, 1976 J. Chem. Phys. 65, 3108-17.
- Lemmens L F and Devreese J T, 1973 Solid State Commun. 12, 1067-9.
- Macfarlane R M and Shelby R M, 1984 Opt. Lett. 9, 533-5.
- Orlov M S and Stolov A L, 1975 Opt. Spectrosc. 39, 640-2.
- Pedrini C, McClure D S and Anderson C H, 1979, J. Chem. Phys. 70, 4959-62.
- Pedrini, C, Rogemond F and McClure D S, 1986 J. Appl. Phys. XX, XXXX.
- Reisfeld R and Jorgensen C K, 1977 Lasers and Excited States of Rare Earths (New York, Springer-Verlag).
- Rotenberg M, Bivins R, Metropolis N and Wooten J K, 1959 The 3-j and 6-j Symbols (Cambridge, Technology Press).
- Struck C W and Fonger W H, 1975 J. Luminesc. 10 1-30.
- Sturge M D, Guggenheim H J and Pryce M H L, Phys. Rev B 2, 2459-71.
- Valyashko E. G, Bodrug S N, Mednikova V N and Smirnov V A, 1977 Opt. Spectrosc. 42, 174-8.
- Wood D L and Kaiser W, 1962 Phys. Rev. 126, 2079-88.
- Yanase A, 1977 J. Phys. Soc. Japan 42, 1680-6.

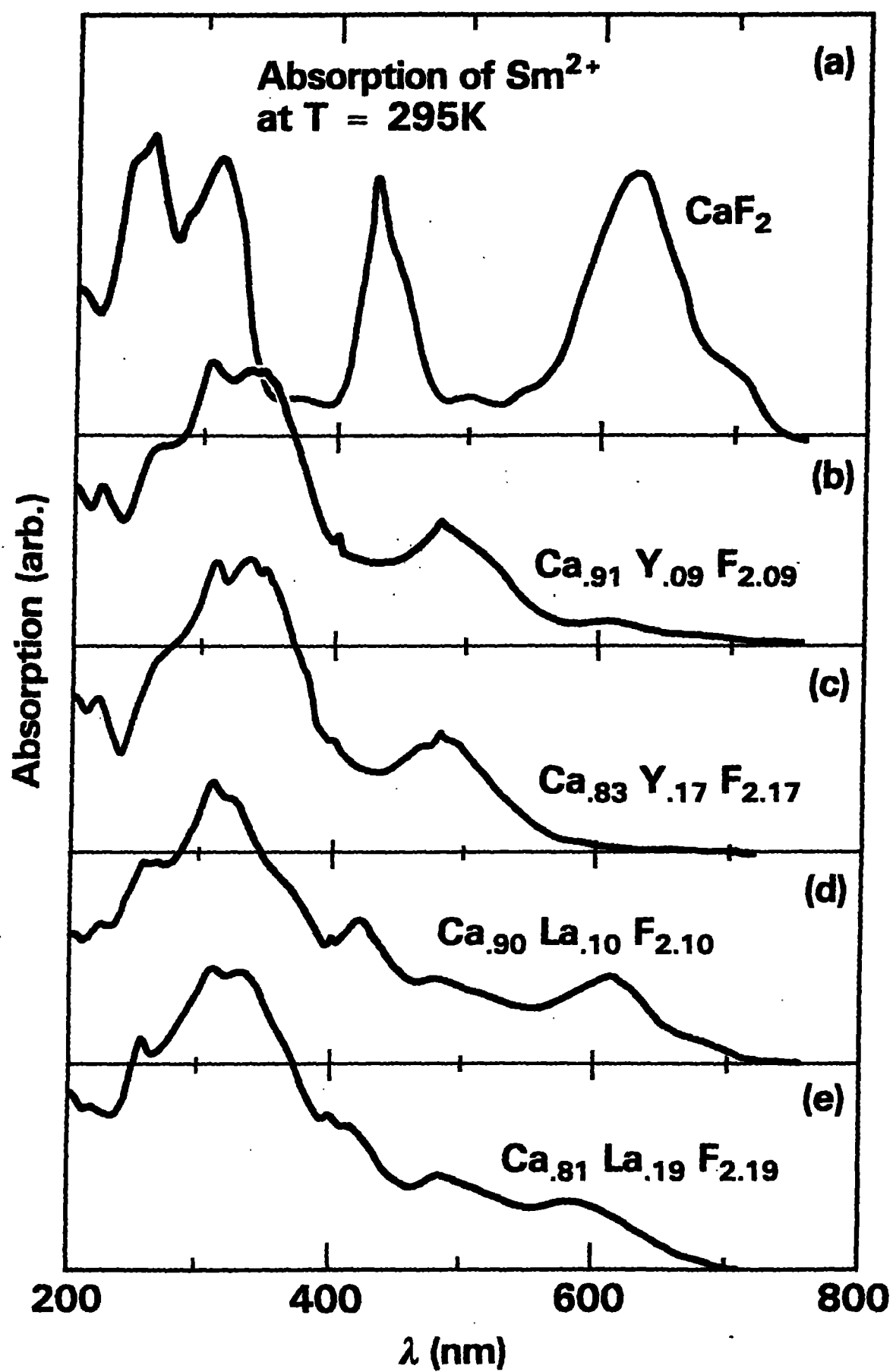


Figure 1

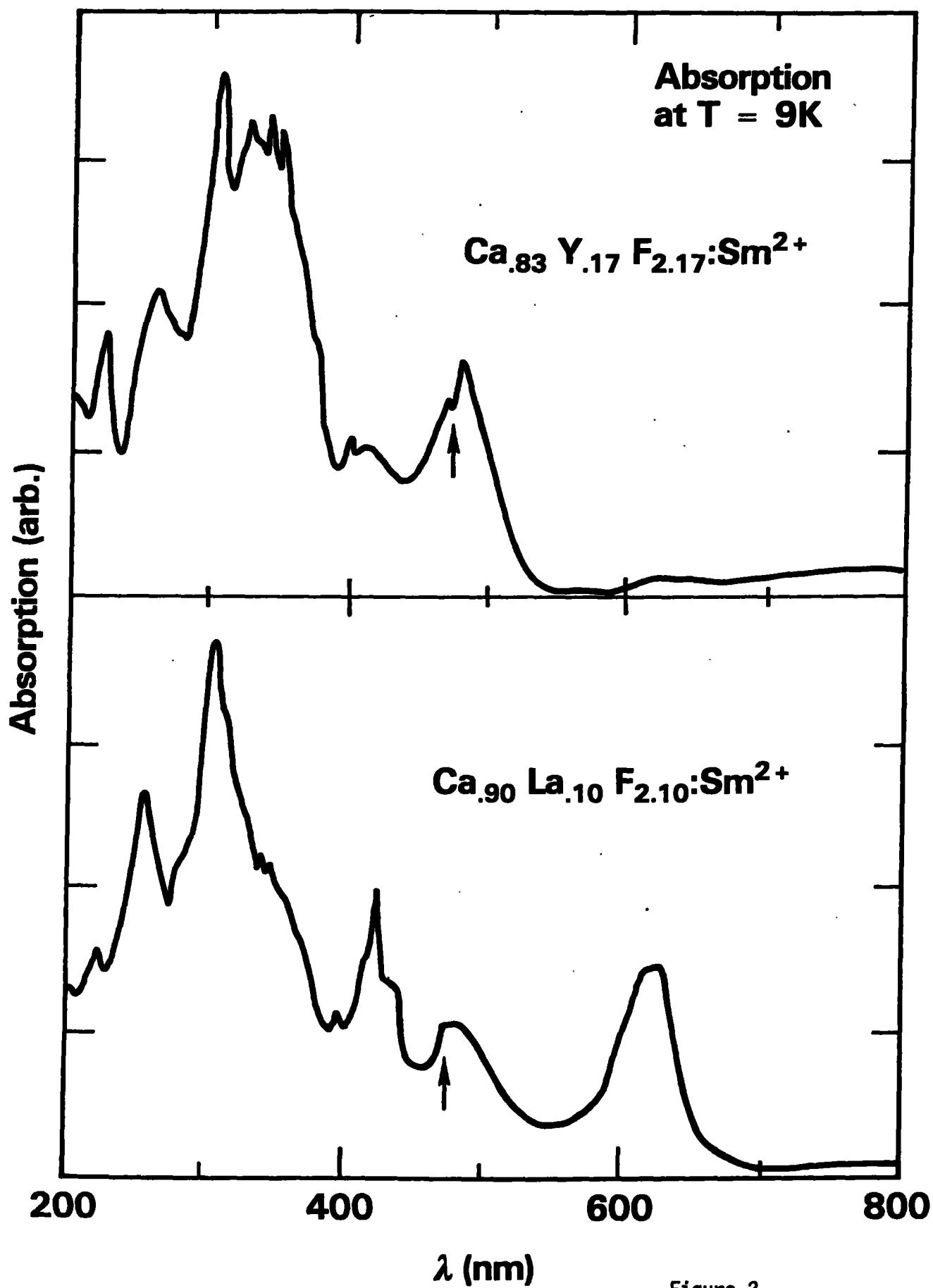


Figure 2

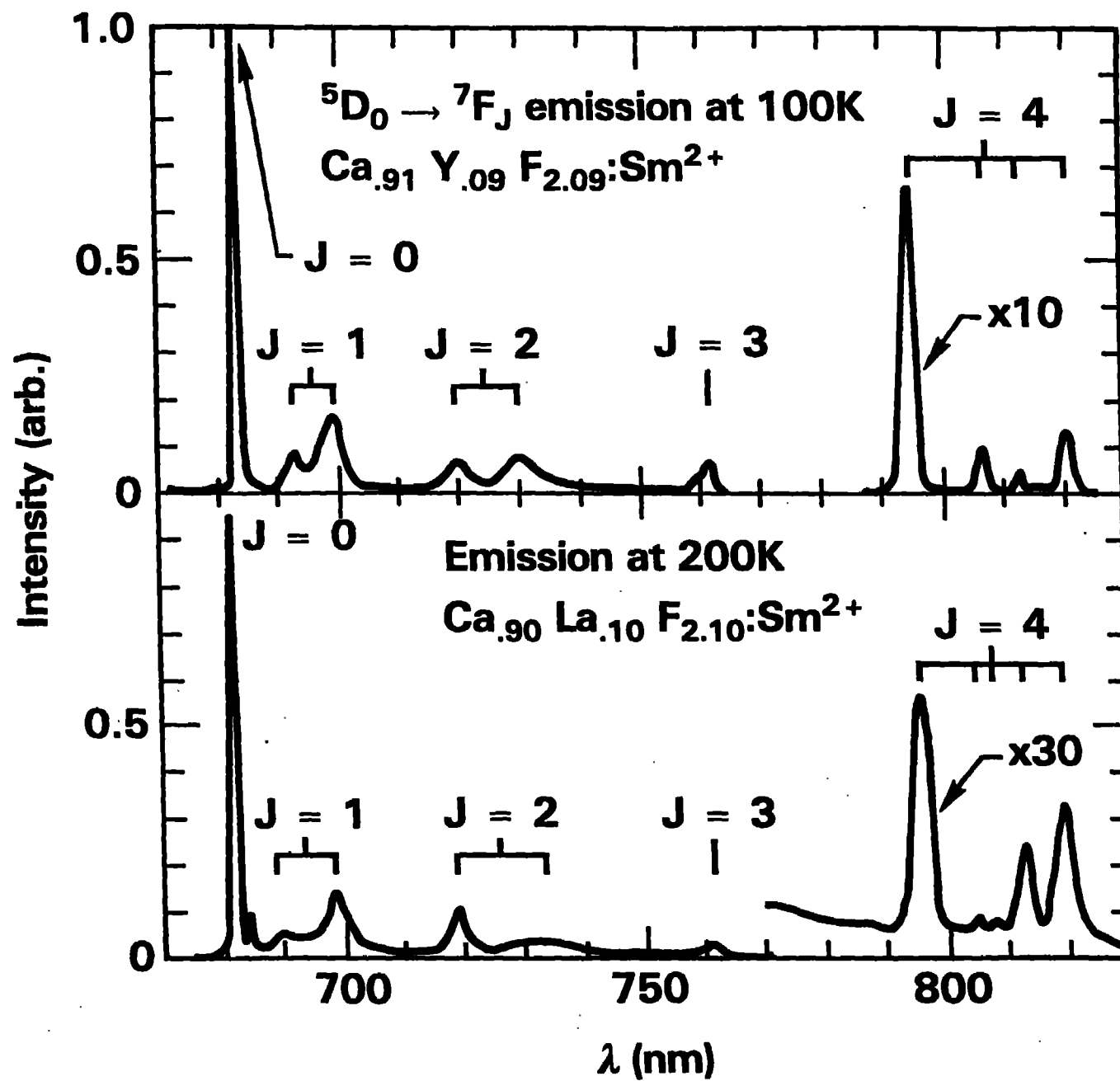


Figure 3

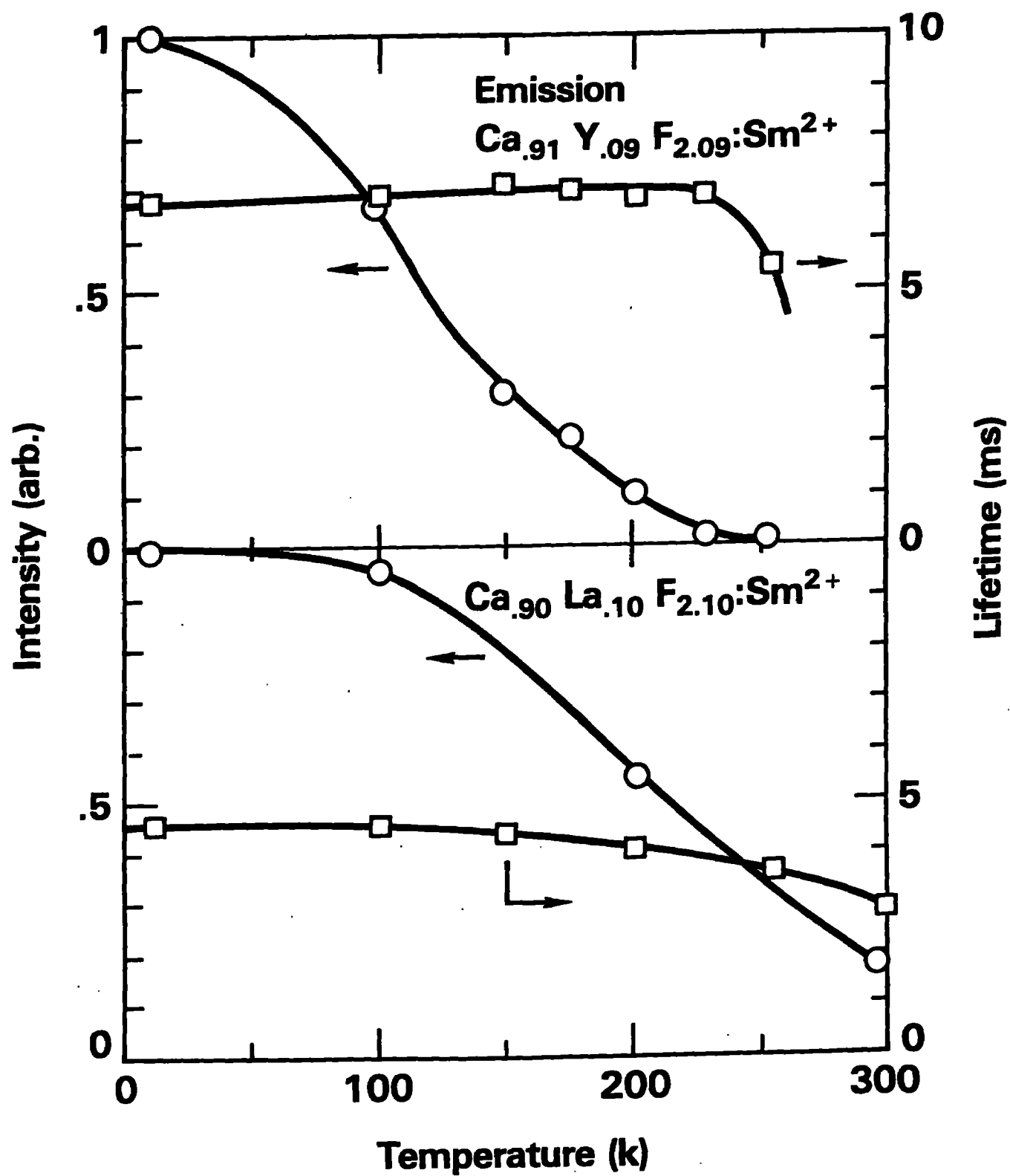


Figure 4

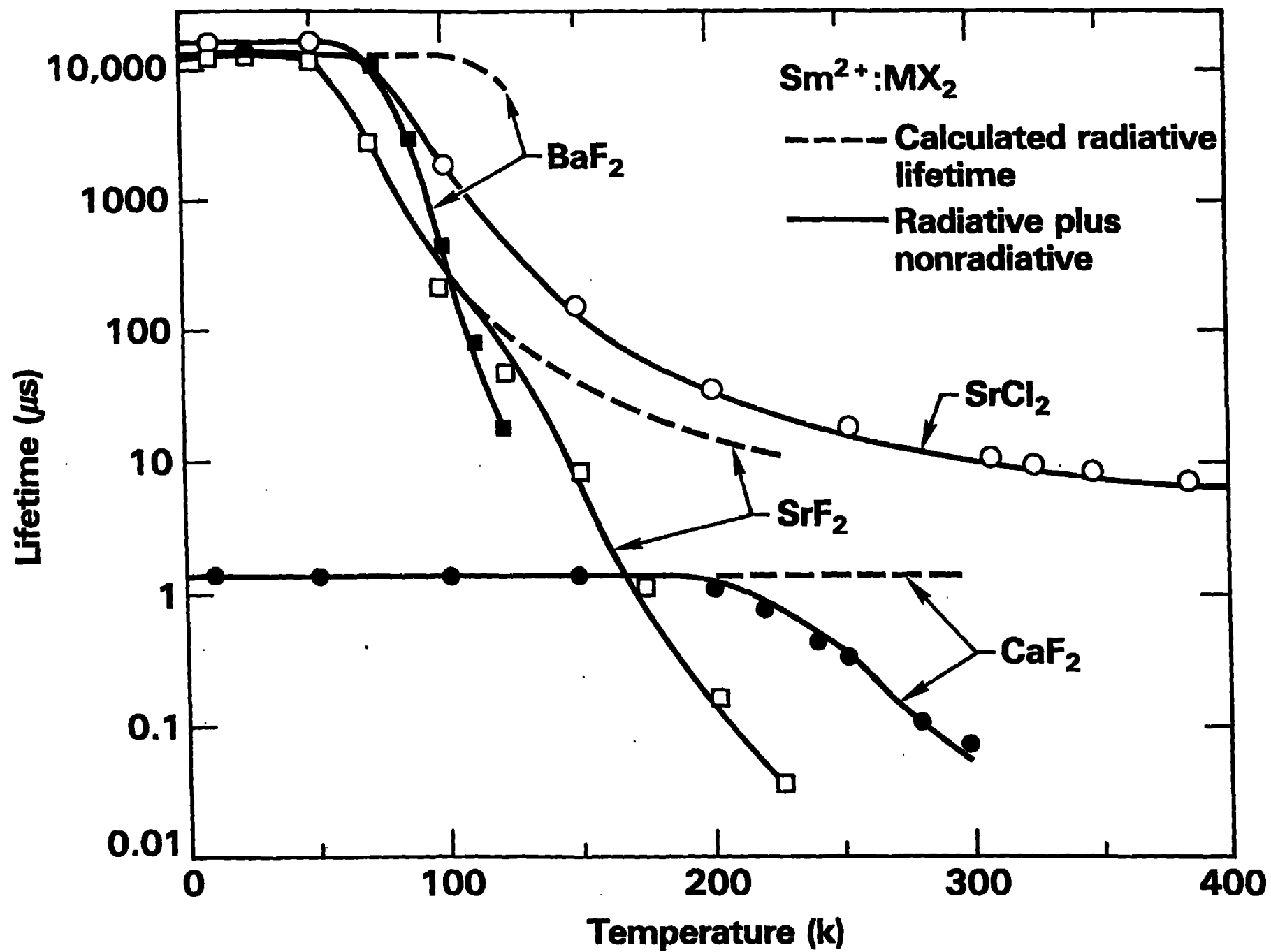


Figure 5